Microelectromechanical Systems

Academic and Research Staff
Professor Dennis M. Freeman, Professor Berthold K. P. Horn, Michael B. McIlrath

Visiting Scientists and Research Affiliates
Dr. C. Cameron Abnet, Abraham R. McAllister, Dr. Michael S. Mermelstein, Dr. Werner Hemmert

Graduate Students
Salil P. Desai, Samson Timoner

Technical and Support Staff
Janice L. Balzer

Sponsors
Defense Advanced Research Projects Agency Grant F30602-97-2-0106
Center for National Research Initiatives Matisse Project
W. M. Keck Foundation Career Development Professorship (Freeman)

1 Computer Microvision for MEMS

Academic and Research Staff
Professor Dennis M. Freeman, Michael B. McIlrath

Visiting Scientists and Research Affiliates
Dr. C. Cameron Abnet, Abraham R. McAllister, Dr. Michael S. Mermelstein, Dr. Werner Hemmert

Graduate Students
Salil P. Desai, Samson Timoner

Technical and Support Staff
Janice L. Balzer

Sponsors
Defense Advanced Research Projects Agency Grant F30602-97-2-0106
Center for National Research Initiatives Matisse Project
W. M. Keck Foundation Career Development Professorship (Freeman)

Introduction

Microelectromechanical systems (MEMS) are fabricated using batch techniques that are similar to those used to fabricate microelectronic devices. Unlike electronics, however, simple methods for testing and characterizing internal failure modes of micromechanical devices do not exist. The major goal of this project is to develop inexpensive and reliable tools for in situ visualization of the motions of internal structures in MEMS by combining light microscopy, video imaging, and machine vision.

Motion measurements with Mirau Interferometric Optics

We have previously demonstrated in situ measurements of 3D motions of MEMS using bright-field microscopy. Images of microelectromechanical systems are magnified with a microscope and projected onto a CCD camera. Stroboscopic illumination is used to take temporal sequences of images at multiple planes of focus. Quantitative estimates of motions are also obtained from the

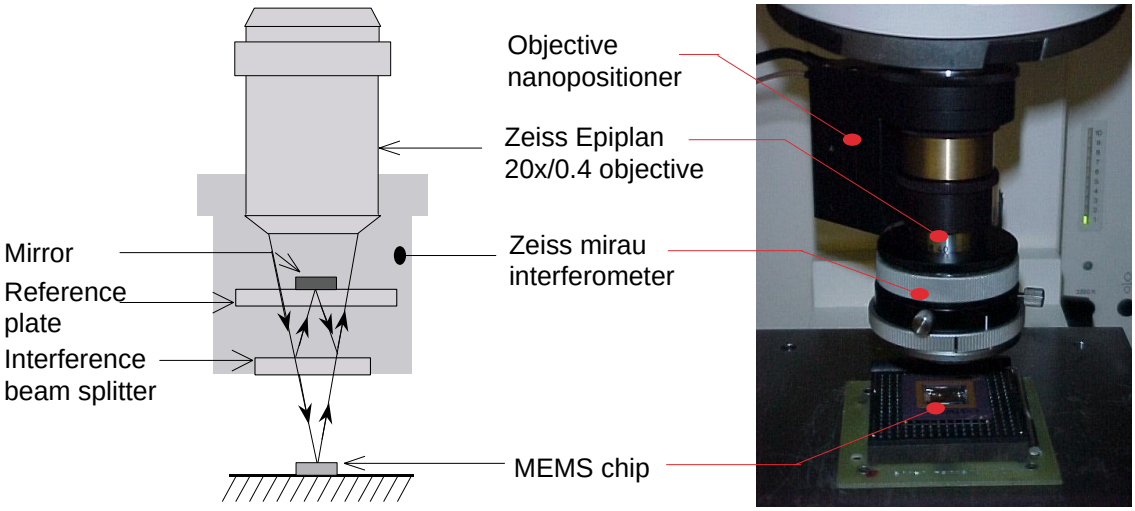

Figure 1: Zeiss Mirau interferometer. Left: Schematic representation. Illumination from the objective is split into two parts by a beam splitter. One part reflects off the MEMS chip and the other part reflects off a mirror on the reference plate. The two parts combine and interfere. Right: Photograph. The Zeiss Mirau interferometer is attached to the microscope through a nanopositioner that translates the interferometer axially.

recorded images using algorithms originally conceived for robot vision.

The resolution of this brightfield measurement system is limited by the numerical aperture of the objective. Nanometer resolutions can be achieved with high quality, long-working distance objectives (Zeiss LD-Epiplan 50x, numerical aperture 0.6). However, in-plane resolution decreases with numerical aperture and out-of-plane resolution decreases with the square of numerical aperture.

Higher out-of-plane resolution can be achieved using interferometric video systems. We have previously demonstrated a Linnik interferometric imaging system with nanometer out-of-plane resolution. This system used custom-fabricated optics, which were difficult and time-consuming to align. We have recently developed a Mirau interferometric video system for measuring three-dimensional motions of MEMS with nanometer precision. The Mirau interferometric system is based on commercial optics that are aligned by the manufacturer and provides out-of-plane resolution comparable to the Linnik interferometer.

The Mirau interferometer (Zeiss Corporation, Germany) consists of a beamsplitter and reference mirror that are packaged into a single unit (Figure 1, right panel) that mounts directly on a long working-distance objective (Zeiss LD-Epiplan 20x). Control knobs allow fine adjustment of the relative optical path lengths. Furthermore, the reference mirror can be rotated out of the beam path so that both brightfield and interference images can be obtained. The Mirau interferometer is attached to the microscope turret via an objective nanopositioner (P720, PIFOC, Polytec PI, Germany). Motions of the nanopositioner alter the optical path length to the target relative to the optical path length to the reference mirror. Interferograms obtained at multiple positions of the nanopositioner are analyzed to determine axial motions of the target in terms of known displacements of the nanopositioner.

Stroboscopic illumination is used to take stop-action interferograms and stop-action brightfield images at multiple phases of periodically driven motions of the MEMS device under test. Illumination is generated using an array of seven LEDs (C505-CB290-E1000, Cree Research Inc., USA). The fast optical rise time of the LEDs (30 ns) allows stop action motion analysis at frequencies up to tens of MHz. The optical bandwidth (50 nm centered at λ = 505 nm) produces light with a coher-

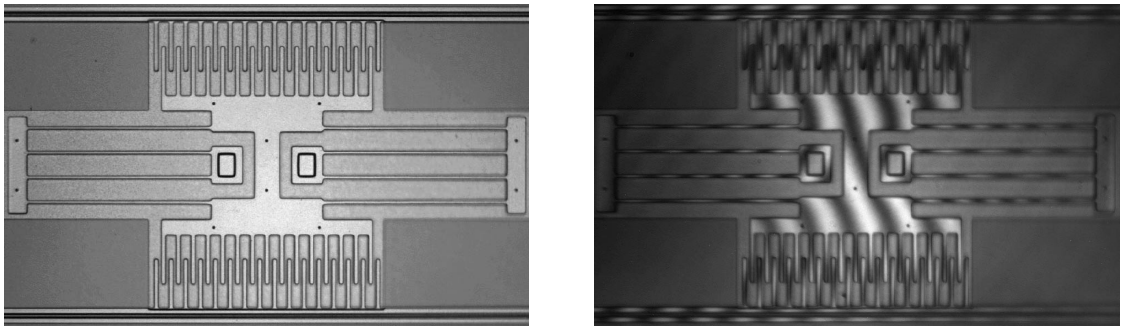

Figure 2: Brightfield and Mirau Interferometric images of a lateral resonator. Both images were obtained using the apparatus described in figure 1. The brightfield image (left) was obtained with the reference mirror rotated out of the optical path. The interferometric image (right) was obtained with the reference mirror rotated into the optical path.

ence length of approximately 15 μm. Thus, interferometric data can be obtained from structures with heights within a 7 μm range. The stroboscopic interferograms were analyzed to determine out-of-plane (z) displacement. The brightfield images were analyzed to determine in-plane (x and y) displacement. Thus the combination of stroboscopic interferograms and brightfield images allows three-dimensional motion analysis.

To demonstrate the motion measurement system, a surface micromachined lateral resonator (fabricated with the MUMPs process, Cronos Integrated Microsystems, USA) was electrically stimulated with a sinusoidal voltage (10 Vp-p AC plus 50 V DC bias) applied to one of the comb drives and the shuttle mass was connected to ground. The system was placed on a vibration isolation table and in an enclosure to minimize the effects of external vibrations and air currents. Brightfield images and interferograms (Figure 2) were obtained at 8 evenly spaced phases of motion and recorded with a CCD camera (Pulnix 1010, Pulnix Inc., USA). For three-dimensional interferometric analysis, interferograms at nine planes of focus (separated by 30 nm) and one brightfield image (at the plane of best focus) were obtained for 8 stimulus phases at each of 33 frequencies (from 1 kHz to 50 kHz).

For three-dimensional brightfield analysis, brightfield images at 10 planes of focus separated by 2 μm were obtained for the same stimulus conditions as the interferograms. The brightfield images were analyzed using Computer Microvision algorithms for comparison with results obtained using stroboscopic interferometry. The noise floor of the system was determined by repeating the same measurements and analysis for images obtained with the stimulus switched off.

In-plane results are shown in figure 3. For the regions of interest analyzed, a second order resonance was detected at 23 kHz in the x-direction (figure 3, left panel). The quality factor (Q) was determined to be 40.8 and the noise floor was 0.4 nm. As expected from the design of the device, motions in the y-direction (figure 3, right panel) are small and comparable to the noise floor (0.6 nm) outside of resonance; the larger amplitude of motion at resonance is due to slight misalignment between the device and camera axes.

Interferometric measurements of out-of-plane motions (figure 4, left panel) demonstrated a second-order resonant frequency at 28.75 kHz, which was more highly damped with Q=2.75. The noise floor for the measurement was 0.4 nm. Brightfield measurements of out-of-plane motions are similar to the interferometric measurements, but the noise floor is 10 times greater.

The results obtained with the Mirau interferometer are comparable to those previously obtained for a Linnik interferometer. Both interferometric systems provide much higher out-of-plane resolution than is possible from brightfield image analysis. Out-of-plane resolution from brightfield images de-

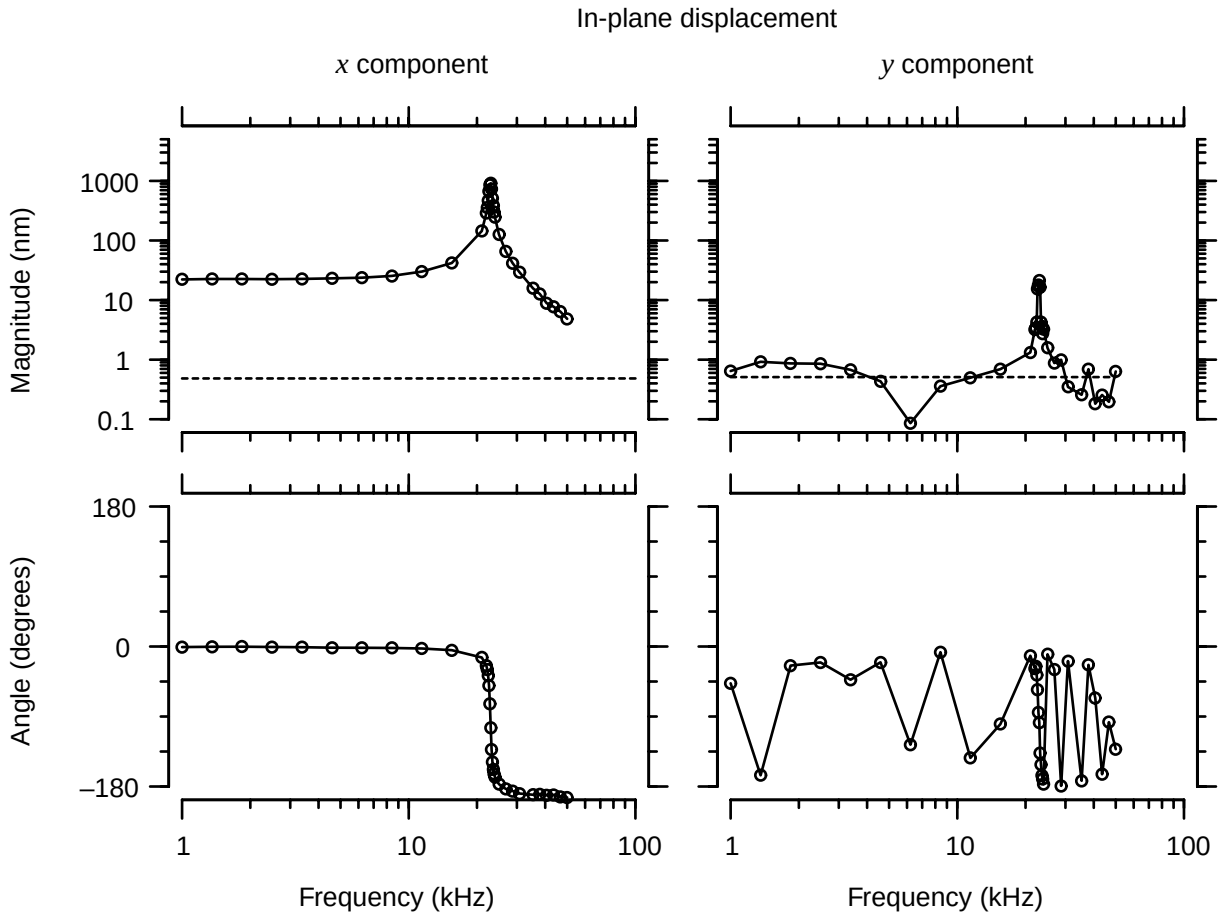

Figure 3: In-plane displacements. The symbols represent the magnitudes (top panels) and angles (bottom panels) of displacements in the intended direction of motion (x, left panels) and in the orthogonal in-plane direction (y, right panels) obtained from analysis of brightfield images. The dashed lines in the top panels show measurements of the noise floor, which is approximately 0.4 nm for the x component and 0.6 nm for the y component.

pends critically on the out-of-plane resolution of the objective. Thus, high resolution requires optics with high numerical aperture. Out-of-plane motions measured interferometrically do not require high resolution objectives. Generally, high numerical aperture can only be achieved for objectives with high magnifications. The higher the magnification, the smaller the field of view, given the same camera. Thus both interferometric systems provide greater fields of view than a brightfield system with comparable out-of-plane resolution.

The principal disadvantage of the Mirau interferometer is that it greatly reduces the working distance of the optical system. The long-working distance objective that we used has a working distance of 9.8 mm which accommodates the integration of other pieces of experimental apparatus such as electrical probes or vacuum fixtures. The beam splitter and reference mirror in the Mirau interferometer reduce the working distance to 1.75 mm. This smaller working distance restricts experimental setup in that parts must typically be wire-bonded and the structures to be measured should be near the surface of the package. By contrast, a Linnik interferometer using the same objective would provide the full 9.8 mm of working distance.

The principal advantage of the Mirau interferometer is that the manufacturer performs the optical alignment. Alignment of the previously designed Linnik interferometer was complicated by the

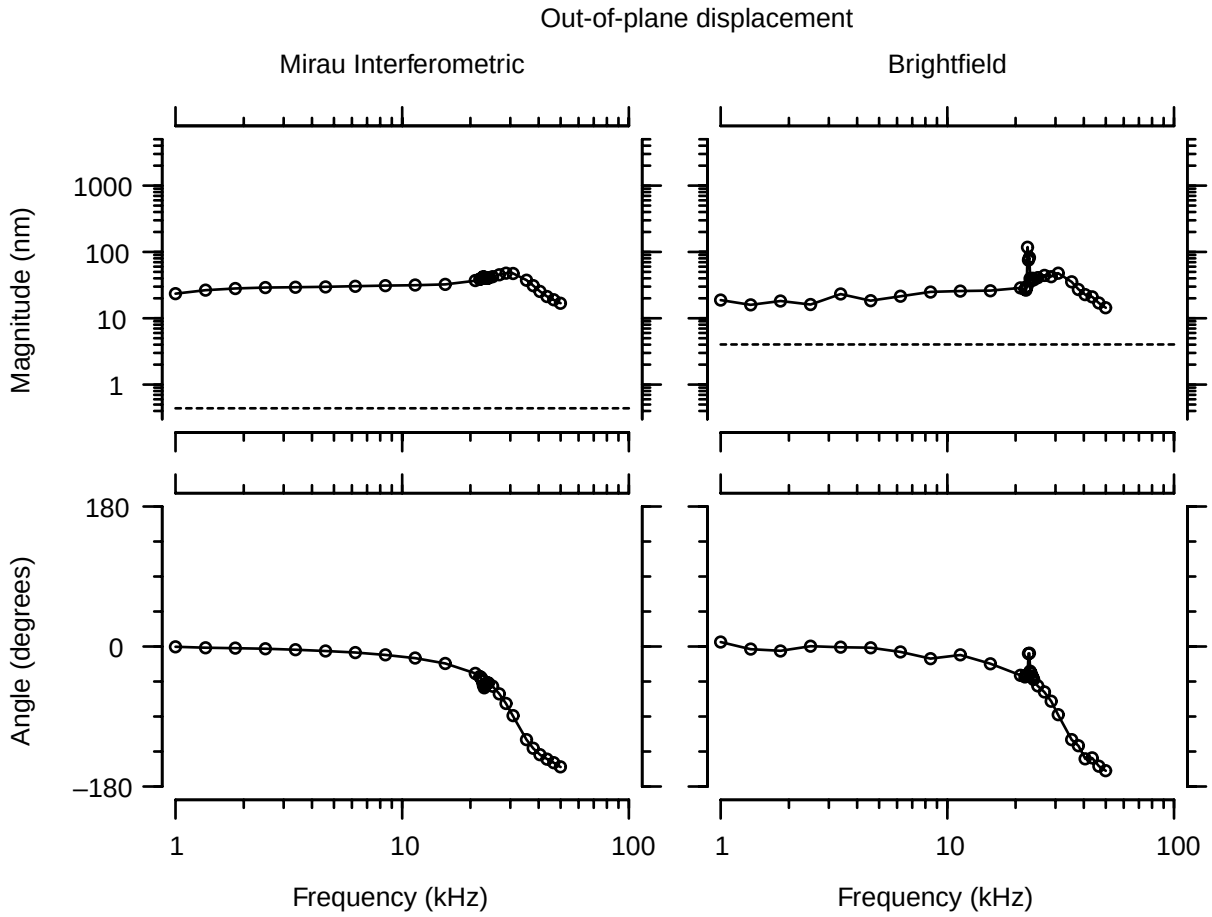

Figure 4: Out-of-plane displacements. The symbols represent the magnitudes (top panels) and angles (bottom panels) of out-of-plane displacements determined by analysis of interferometric images (left panels) and by analysis of brightfield images (right panels). The dashed lines in the top panels show measurements of the noise floor, which is approximately 0.4 nm for the interferometric measurement and 4 nm for the brightfield measurement.

short coherence length of the LED light source (approximately 15 μm). This required the optical path lengths to the target and reference mirror to be matched to within 15 μm. Focusing the target while maintaining the optical paths to this precision was difficult and tedious. By contrast, the Mirau interferometer obviates the need for precision alignment. The results obtained with the Mirau interferometer demonstrate the combination of the superior axial resolution of interference methods with the superior lateral resolution of computer microvision to achieve three-dimensional motions with greater precision and ease.

Published papers

Journal Articles Published

Timoner, S.J. and Freeman, D.M. “Multi–Image Gradient-Based Algorithms for Motion Estimation.” *Optical Engineering*, in press.

Freeman, D.M. “Measuring Motions of MEMS.” *MRS Bulletin*, in press.

Meeting Papers Published

Desai, S.P. and Freeman, D.M. “Nanometer Resolution of Three- Dimensional Motion using Mirau Interferometric Optics.” *Proceedings of the International iMEMS Workshop 2001*, Singapore, July 2001.

2. Synthetic Aperture Lithography

Academic and Research Staff
Professor Dennis M. Freeman, Professor Berthold K. P. Horn

Visiting Scientists and Research Affiliates
Lightwave Instruments, LLC

Graduate Students
Stanley Hong, Jekwan Ryu

Technical and Support Staff
Janice L. Balzer

Sponsors
Defense Advanced Research Projects Agency Grant N66001-00-1-8908
W. M. Keck Foundation Career Development Professorship (Freeman)

Introduction

The goal of this project is to develop Synthetic Aperture Lithography (SAL), a powerful new paradigm for optical lithography that promises

- lensless and maskless projection of arbitrary patterns,
- multiple-wavelength depth of field, and
- sub-100 nm critical dimensions using conventional light sources and resist chemistries.

In traditional optical lithography, light from an illuminator passes through a mask and is focused by a lens to recreate the mask pattern on a wafer. SAL replaces the lens, the mask, and the mask illuminator with a discrete set of controllable source beams that emulate key control points in this field. Within their region of overlap on the wafer, a small number (n) of beams produces images with a much larger number (n^2) of Fourier components. Therefore, complex patterns can be projected with 15 to 100 beams. Furthermore, by sensing the amplitude, phase, and direction of each beam, feedback control can be used to compensate for mechanical imperfections in the projection apparatus and for disturbances in the environment, such as substrate vibration. Thus electronic feedback in SAL substitutes for physical perfection in traditional optical lithography. Similarly, by sensing the positions of previously patterned structures, the projected image can be aligned actively to those structures.

Surface Acoustic Wave Optical Modulation

The Synthetic Aperture Lithography project builds on our previous efforts to develop a Synthetic Aperture Microscope. In that project, we split the beam of a 488 nm argon ion laser into as many as 100 beams using an acousto-optic modulator (AOM). The amplitude and phase of each beam was independently controlled by modulating the RF signal driving the AOM.

We are developing an all-reflective, MEMS-based, optical modulator. An all-reflective modulator could in principle work for shorter (ultraviolet) wavelengths for which refractive optics are precluded by the lack of suitably transparent materials. One approach to implementing an all-reflective light modulator is to use surface acoustic waves to corrugate the surface of a mirror.

A series of surface acoustic wave optical modulators (SAW-Mods) were fabricated by patterning deposited aluminum on substrates of lithium niobate using standard photolithographic techniques. Each SAW-Mod explored a different transducer design or operating center frequency. This past

year, the optical performance of each SAW-Mod was tested. Technical issues included the construction of custom RF matching circuitry and the attenuation of standing wave patterns. Using a 633 nm HeNe laser at normal incidence, diffraction angles of 0.21 and 0.32 degrees were measured for SAW-Mods with center frequencies of 19.77 and 29.66 MHz, respectively. The maximum diffraction efficiency obtained during testing was 2.1%. These results agreed with theoretical predictions.

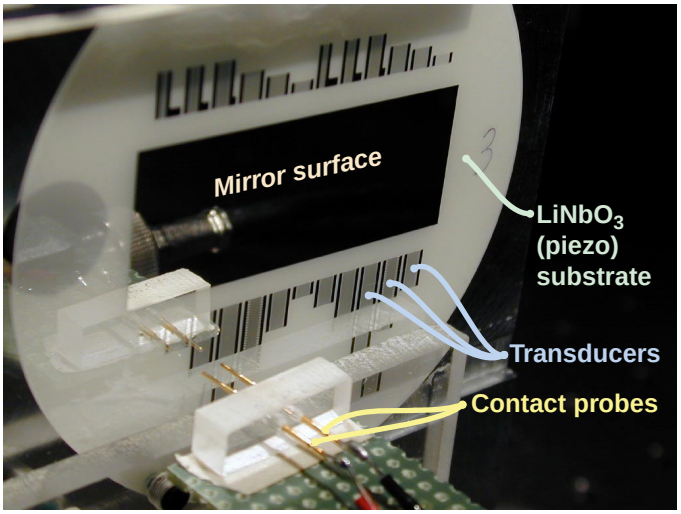

Figure 5: A wafer of SAW-Mods. The rectangular region in the center of the wafer is the SAW-Mod mirror. The vertical strips directly above and below the mirror are 24 individual interdigital transducers. The wafer is held in a mount made from aluminum and cast acrylic and secured with nylon-tipped screws. A dual spring-loaded contact probe assembly used to connect a transducer to a BNC cable is visible in the foreground.

Published papers

Theses

Hong, S.S., “Surface Acoustic Wave Optical Modulation.” M.Eng Thesis, Department of Electrical Engineering and Computer Science, M.I.T., February 2001.